Journal of Magnetism and Magnetic Materials 505 (2020) 166676

Contents lists available at ScienceDirect

Journal of Magnetism and Magnetic Materials

journal homepage: www.elsevier.com/locate/jmmm

Research articles

Effects of Fe substitution on Mn_2Sn alloy on its structural, magnetic and magnetocaloric properties

Marissol R. Felez[a,*], José Carlos B. Monteiro[a,d], Daniel Z. de Florio[b], Flavio C.G. Gandra[a], Sergio Gama[c]

[a] Universidade Estadual de Campinas, Instituto de Física Gleb Wataghin, Campinas, SP 13083-859, Brazil
[b] Universidade Federal do ABC, Centro de Engenharia, Modelagem e Ciências Sociais Aplicadas, São Paulo, SP 09210-580, Brazil
[c] Universidade Federal de São Paulo, Departamento de Ciências Exatas e da Terra, Diadema, SP 09910-720, Brazil
[d] Universidade Federal do Maranhão, Centro de Ciências Sociais Saúde e Tecnologia (CCSST), Imperatriz, MA 65900-410, Brazil

ARTICLE INFO

Keywords:
Magnetic measurements
Biphasic material
Layered material
Magnetic refrigeration
Thermomagnetic motors

ABSTRACT

The effects of Fe substitution on Mn site of Mn_2Sn compound was investigated by means of scanning electron microscopy with X-ray energy dispersive spectrometer, X-ray diffraction, magnetization and magnetocaloric measurements. The produced $Mn_{2-y}Fe_ySn$ series ($0.50 \leq y \leq 1.75$) presented two phases, a major non-stoichiometric $Mn_{2-x}Sn$ and a minor Mn_3Sn, respectively, with Fe content replacing Mn in each phase. The lattice parameters *a* and *c* of $Mn_{2-x}Sn$ and Mn_3Sn phases decrease approximately linearly with Fe concentration while their transition temperatures increase covering a wide temperature range from 177 K to 546 K (major phase T_{C1}) and 260 K to 704 K (minor phase T_{C2}) resulting in alloys with two distinct values of T_C. The magnetization measurements show a ferromagnetic coupling and saturation magnetization increases along the series. The heat flux analyses determined second order of magnetic transitions and magnetocaloric effect was calculated with $|\Delta S|$ around 1 J/kg.K. The cooling power was estimated in 85 J/kg. Both values were for $\mu_0\Delta H = 2$ T. Thereby, for technological devices which have their efficient improved using layered materials, $Mn_{2-y}Fe_ySn$ alloys are valid candidates since the association of its properties allow to yield a powerful magnetic and magnetocaloric material, and, besides, they are low cost, non-toxic, absent of rare-earth and easy to manufacture.

1. Introduction

Mn-based compounds have been considered as promising materials [1–4] for magnetic refrigeration [5,6], either because Mn has the highest magnetic moment among 3d transition elements [4] or because it is abundant on Earth's crust making it cheaper than rare-earth elements and less impactful to the environment. Some studies have investigated the crystalline, magnetic and magnetocaloric properties of Mn-Fe-Sn ternary materials with Ni_2In ($B8_2$) type structure [7] and hexagonal $P6_3/mmc$ symmetry such as $(Mn_{1-x}Fe_x)_7Sn_4$ [8], $(Mn_{1-x}Fe_x)_{65}Sn_{35}$ [9], $Mn_{1.66}Fe_{0.02}Sn$ [10], $(Mn_{1-x}Fe_x)_5Sn_3$ [11], $Mn_{1.5}M_{0.5}Sn$ (M = Cr, Mn, Fe, Co) [12] and $Fe_{5-x}Mn_xSn_3$ [13]. One of the key features of those compounds is that their magnetic properties are easily adjusted by the concentration of its elements and, as so, they can be rather useful in order to develop materials with targeted applications, such as thermomagnetic motors [14–21] or magnetic refrigerators [22,23]. Regarding those technologies, recent research shows the importance of table-like magnetocaloric effect (MCE) encompassing large temperature ranges arising from layered [24,25] and composite [26–28] magnetocaloric materials.

According to Mn-Sn phase diagram [29], the Mn_2Sn alloy (in the nominal stoichiometry of 66.7 at.% Mn) at 800 °C, presents itself in a biphasic field of compositions, with coexistence of both the Mn_3Sn phase and a non-stoichiometric $Mn_{2-x}Sn$ phase, where the latter is predominant by the lever rule. The $Mn_{2-x}Sn$ is a high temperature phase that synthetizes within a variable stoichiometry where the amount of Mn can vary from 65 at.% at 480 °C to 68 at.% at 884 °C. Due to this feature the synthesis of a single phase $Mn_{2-x}Sn$ is very unlikely to occur and a small quantity of the Mn_3Sn phase is expected to parasite any attempt of growth the $Mn_{2-x}Sn$ phase.

$Mn_{2-x}Sn$, Ni_2In-type [8,9,30–33], and Mn_3Sn, Ni_3Sn-type [34–49], compounds have been reported as ferrimagnetic and antiferromagnetic phases, respectively, with non-collinear magnetic ordering which usually involves competition between (ferro/ferri)magnetic and antiferromagnetic exchange interactions between Mn moments, located at different lattice sites. Consequently, the $Mn_{2-x}Sn$ phase has low

* Corresponding author.
E-mail address: mrfelez@ifi.unicamp.br (M.R. Felez).

https://doi.org/10.1016/j.jmmm.2020.166676
Received 10 February 2020; Accepted 27 February 2020
Available online 28 February 2020
0304-8853/

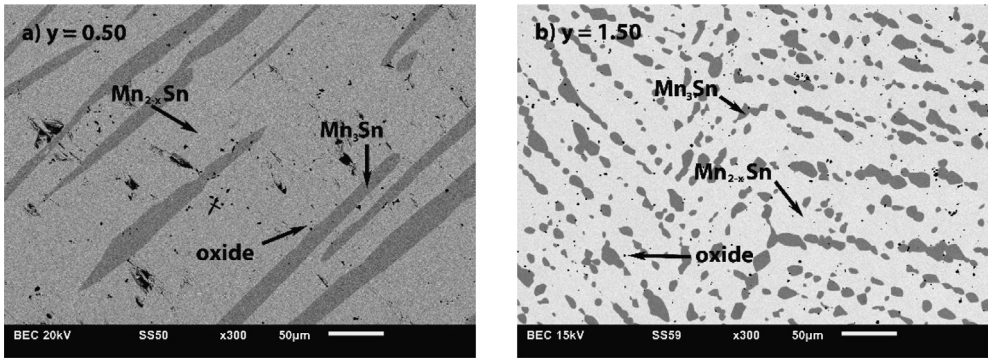

Fig. 1. Backscattered SEM images and observed phases for the samples with: (a) y = 0.50, (b) y = 1.50.

saturation magnetization moment and a usually complex magnetic ordering. It is supposed that replacing Fe, in the Mn sites, should increase the number of ferromagnetically coupled Fe-Fe or Fe-Mn pairs, breaking the antiferromagnetically coupled Mn-Mn element [12] and giving rise to a ferromagnetic ordering, since Fe element has ferromagnetic state. Besides that, Fe radius is smaller than Mn, promoting an easy substitution of Fe in the same site occupied by Mn and decreasing the interatomic distance.

In this work we propose a systematic study of the effects of the Fe substitution at the Mn site of the $Mn_{2-y}Fe_ySn$ alloy, in the $0.50 \leq y \leq 1.75$ range, in order to explore the combination of factors as the low cost and environmental impact of Mn-Fe-Sn system and the possibility of producing a material with easily tunable magnetic properties for new technologies. The phase relations and crystallographic data will be analyzed by EDS and XRD techniques, and the system magnetic, calorimetric and magnetocaloric properties will be obtained and discussed as follows.

2. Materials and method

$Mn_{2-y}Fe_ySn$ ($0.50 \leq y \leq 1.75$, with $\Delta y = 0.25$) polycrystalline samples were prepared from high purity elements (> 99.99%). Each composition was melted in an arc-furnace under high purity argon atmosphere. Molten buttons were turned and re-melted at least three times to ensure homogeneity. Samples were encapsulated in a high purity argon atmosphere, heat-treated at 800 °C for 10 days and subsequently water quenched. Samples were characterized by Scanning Electron Microscopy (SEM) and X-Ray Diffraction (XRD). Scanning electron micrographs were obtained in a JEOL JSM-6010LA equipped with an Energy Dispersive Spectrometer (EDS) used to obtain an atomic semi-quantitative analysis. The XRD diffractograms were obtained with a Bruker D8 Advance AXS X-ray diffractometer using CuKα radiation and a NiKβ filter. Refinement was performed with the aid of the Bruker AXS's TOPAS 4.2 software by Rietveld method.

Magnetic and magnetocaloric effect measurements were carried out in a Quantum Design Magnetic Properties Measurement System (QD-SQUID MPMS) while specific heat was evaluated using a Peltier setup in a Physical Properties Measurement System (QD-PPMS). Peltier element works as a heat flux sensor and measures the amount of heat that goes through the sample using the reliable temperature and magnetic field platform provided by the PPMS. Rectangular pieces (m ≈ 500 mg, length ≈ 7 mm, width ≈ 5 mm and thickness ≈ 2 mm) of Mn-Fe-Sn samples were cut and glued on the top plate of the Peltier using a thermal conducting epoxy. Measurements were made from 20 K to 330 K under magnetic fields up to 5 T. Further experimental details about the setup are at [50,51].

3. Results and discussion

3.1. SEM and EDS results

Full set of backscattered SEM images revealed that $Mn_{2-y}Fe_ySn$ alloys are homogeneous for all y values: all the images show essentially two distinct areas with different tones of gray with some small scattered black dots. The EDS results proved the Fe presence in both areas and provided the average values of Mn, Fe and Sn concentration. For the light gray area, it was found that the average sum of the values for Fe and Mn concentrations resulted in values 2 times the Sn content, $(MnFe)_{2-x}Sn$, maintaining the 2 to 1 stoichiometric ratio observed in primitive $Mn_{2-x}Sn$ phase. For the dark gray zones, the average sum of Mn and Fe concentrations is 3 times the Sn content, $(MnFe)_3Sn$, also preserving the 3 to 1 stoichiometric ratio observed in original Mn_3Sn phase. In all samples, for both phases, the fully substitution of Mn by Fe was not observed and the Mn-Fe ratio was very close to the nominal. Black spots are minor oxides found within the samples and were not counted as a third phase.

From the microscopy analysis, it is very clear that the major phase within these samples is the $Mn_{2-x}Sn$ phase with a smaller and variable amount of a minor Mn_3Sn phase, regardless the Fe content. Some of the SEM images obtained are shown in Fig. 1a and b, for samples with y = 0.50 and 1.50. Two distinct phases are observed, the $Mn_{2-x}Sn$ and Mn_3Sn, both with Fe presence as indicated by EDS analysis.

Henceforth, $Mn_{2-x}Sn$ and Mn_3Sn phases will be referred to as 2:1 and 3:1 phases, respectively.

3.2. XRD results

Rietveld refinements were performed for the $Mn_{2-y}Fe_ySn$ system always following the same refining strategy. Ni_2In-type hexagonal structure (ICSD No. 104976) corresponding to 2:1 phase and Ni_3Sn-type hexagonal structure (ICSD No. 104978) related to 3:1 phase, both with the same $P6_3/mmc$ space group, provided a good fit in all samples. Quantitative Phase Analysis, (QPA), performed by Rietveld refinement, indicate that 2:1 phase appeared in major amount, in agreement with SEM images and EDS results. Lattice parameters *a* and *c* of 2:1 and 3:1 crystalline structures were calculated by Rietveld refinement for the samples and their dependence with Fe concentration is shown in Fig. 2a and b. Since Fe atomic radius is smaller than the Mn, both *a* and *c* decrease with increasing y, as expected.

3.3. Magnetization

Magnetization behavior as a function of the temperature of the $Mn_{2-y}Fe_ySn$ system is shown at Fig. 3, where we observe that all samples presented more than one magnetic transition. As pointed out by SEM images, EDS and quantitative phase analysis prepared samples have 2:1 as the major phase and as magnetic transitions have ferro-or

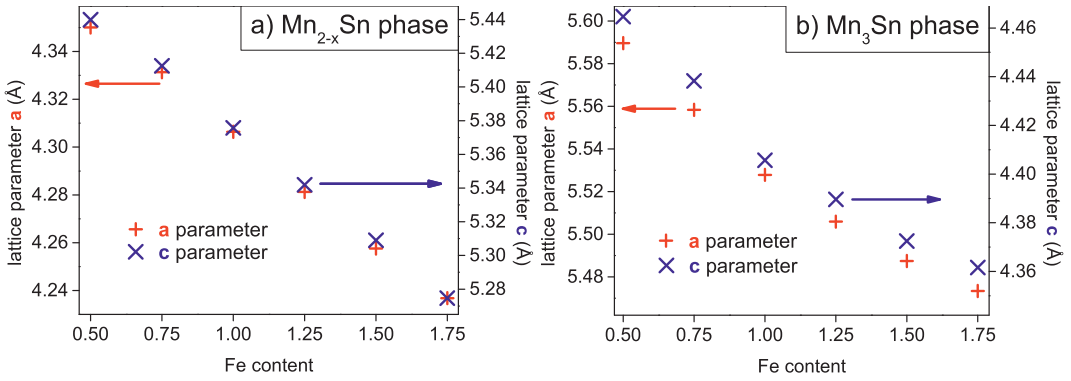

Fig. 2. Fe concentration dependence of hexagonal lattice parameters *a* and *c* (a) for the $Mn_{2-x}Sn$ phase in the $0.50 \leq y \leq 1.75$ range; (b) for the Mn_3Sn phase in the $0.50 \leq y \leq 1.75$ range. The errors bars are shorter than the size of the symbol and because of that they are not pointed on the graphs.

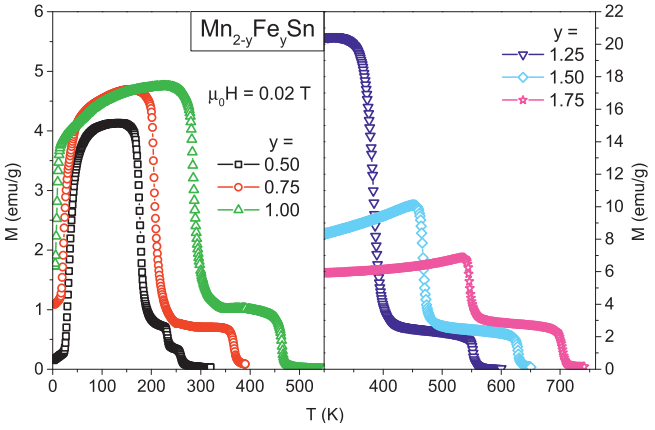

Fig. 3. M(T) curves for the $Mn_{2-y}Fe_ySn$ series obtained under a 0.02 T magnetic field in the ZFC protocol.

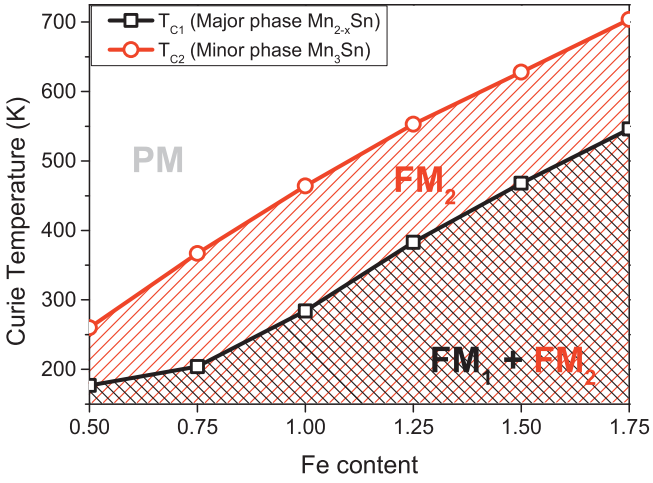

Fig. 4. Magnetic phase diagram encompassing both phases found within our samples. The black and red lines are, respectively, the transition borders of the 2:1 and 3:1 phases and the hatched areas represent the magnetic state of the compounds (PM stands for paramagnetic and FM for ferromagnetic). (For interpretation of the references to colour in this figure legend, the reader is referred to the web version of this article.)

Table 1
Fe concentration dependence of T_{C1} and T_{C2} for $Mn_{2-y}Fe_ySn$ ($0.50 \leq y \leq 1.75$) alloys.

y	0.50	0.75	1.00	1.25	1.50	1.75
T_{C1} (K)	177	204	284	383	468	546
T_{C2} (K)	260	367	464	553	628	704

ferrimagnetic characteristics, we associated the lower Curie (T_{C1}) temperature to the major phase because it should present a greater change to the magnetization. Table 1 shows the Curie temperatures along the series, where T_{C1} stands for the transition temperature of the major phase (lower values) and T_{C2} for the minor phase (higher values). $Mn_{1.50}Fe_{0.50}Sn$ presented three distinct transitions, one very clear, at 177 K, and two others at 233 K and 260 K that could be due to inhomogeneity within the sample as its T_C is very sensible to the lattice position of Mn and Fe atoms [12] and there was not third phase detected by SEM, EDS and XRD analysis. We can also notice that the transition temperatures increase with Fe concentration and neither of those samples presented thermal hysteresis (not show), which could be an indication that the transitions are of second order.

By evaluating the transition temperature of both 2:1 and 3:1 phases found within the samples, we drafted a magnetic phase diagram, shown in Fig. 4. There, white area stands for the paramagnetic (PM) state of both phases, black hatched area represents the ferromagnetic state of the major phase (FM_1) and red hatched area implies the ferromagnetic state of the minor phase (FM_2). Below the black line (T_{C1} values), both phases are FM and their magnetization overlaps. Looking at the phases delimiting curves, we observe that both transition temperatures increase monotonically towards higher Fe concentration. The 2:1 phase presents a slow T_C increase at low Fe concentration followed by an almost linear behavior towards $Mn_{0.25}Fe_{1.75}Sn$ sample while for the 3:1 phase we have a parabolic arc trend towards the Fe side.

An interesting feature of the $Mn_{2-y}Fe_ySn$ system is that the transition temperature presents a large variation with the substitution of Fe for Mn. One can tune the magnetic transition of the major phase over an expressive 369 K range, between 177 K and 546 K, which includes room temperature and its surroundings. This aspect is an advantage because it allows the possibility of creating composites or multilayer compounds to work on cascade thermomagnetic devices such as motors or refrigerators that operate over a wide temperature span. For both phases, these transitions are strongly dependent on alloy composition and are tunable by Fe content.

Fig. 5a shows isothermal M(H) curves for the series, measured at 4 K, where we observe that the saturation magnetization (M_S) increases. This behavior is illustrated in Fig. 5b and although the Fe moment is smaller than the Mn moment, the M_s increase is related to the displacement produced by the Fe atom in the Mn (2d) site, which gradually transforms the ferrimagnetic coupling into a ferromagnetic one, as shown by Shiraishi et al. [9]. Also, for $y \leq 1.00$, the series presents a critical field around 0.25 T. As Fulgsby et al. [12] point out, those Mn based Ni_2In-type compounds usually present Mn-Mn pairs aligned both parallel and antiparallel, depending on which site the Mn occupies. This critical field suggests that the magnetic field can weaken the Mn-Mn

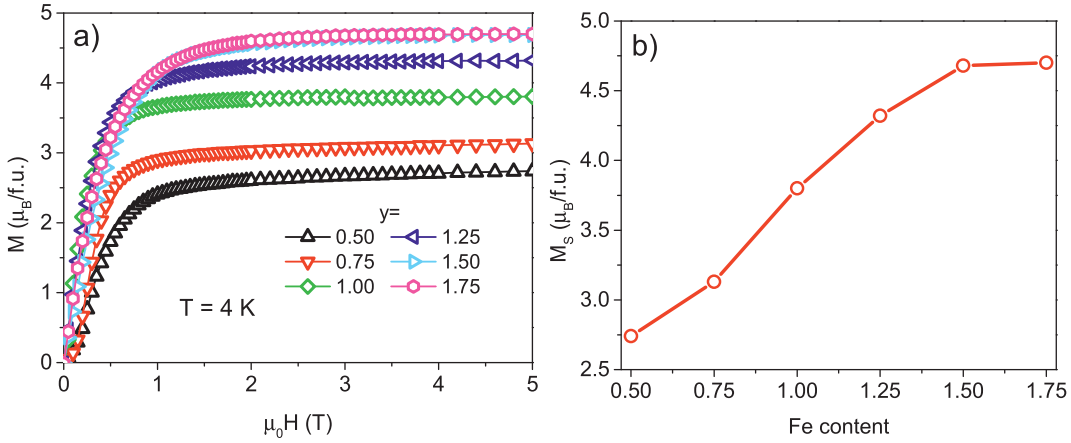

Fig. 5. (a) Isothermals of magnetization M(H) carried out at 4 K up to 5 T, for $Mn_{2-y}Fe_ySn$ ($0.50 \leq y \leq 1.75$) alloys; (b) Saturation magnetization behavior curve, showing a M_s increase up to $y = 1.25$ followed by maximum at $y = 1.75$.

antiparallel pairs turning some of them into a parallel alignment. However, the field does not appear to be enough to completely transform the ferrimagnetic behavior to a ferromagnetic one. Samples with $y \geq 1.50$ seem to have achieved a maximum saturation magnetization which could imply that, at this Fe-Mn ratio, the samples are ferromagnetic. We also measured magnetic hysteresis (not show) of these samples and, up to $y = 0.75$, we observe a coercive field of about 1 kOe that reduces to 0.3 kOe for the $y = 1.00$ sample and subsequently vanishes for the rest of the series.

3.4. Specific heat and magnetocaloric properties

Magnetization measurements showed no thermal hysteresis for those compounds indicating a probable second order magnetic transition (SOMT) and to confirm this hypothesis, we performed heat flux measurements with a Peltier system. The results are shown at Fig. 6a for samples with $y = 0.50$, 0.75 and 1.00 measured under zero magnetic field up to 330 K. As we expected, the transitions are of second order and appear at the curves as a very smooth change in c_P slope for $y = 0.50$ and 0.75 samples and as a broad hill at the $y = 1.00$ alloy.

Magnetic field influence over the specific heat is show at Fig. 6b for samples with $y = 0.75$ and 1.00. Following the characteristics of a SOMT, we observe a broadening of the transition and a shift of T_C to higher temperatures. The effect of the magnetic field, however, is not expressive and we should expect small values arising from the magnetic entropy variation for these compounds. We calculated the ΔS through $M(T)_{(ZFC)}$ curves measured at magnetic fields up to 2 T and the results

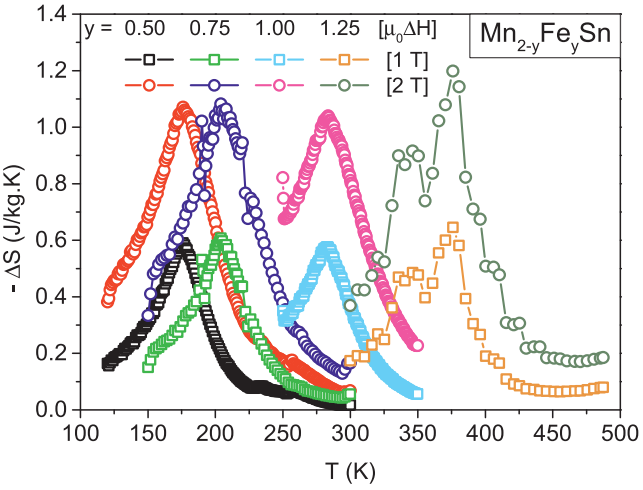

Fig. 7. Temperature dependence of magnetic entropy change, $\Delta S(T)$, for $y = 0.50$, 0.75, 1.00 and 1.25 samples.

are show at Fig. 7 for samples with $0.50 \leq y \leq 1.75$. The values obtained (Table 2) are in agreement with those found for other Mn-Fe-Sn alloys such as the $(Mn_{1-x}Fe_x)_5Sn_3$ [11] and $Mn_{3-x}Fe_xSn_2$ [52] reaching modest values around 1.1 J/kg for a 2 T magnetic field variation. Although the series magnetic entropy variation seems low, in comparison with other materials, if we look to its relative cooling power [53,54] we

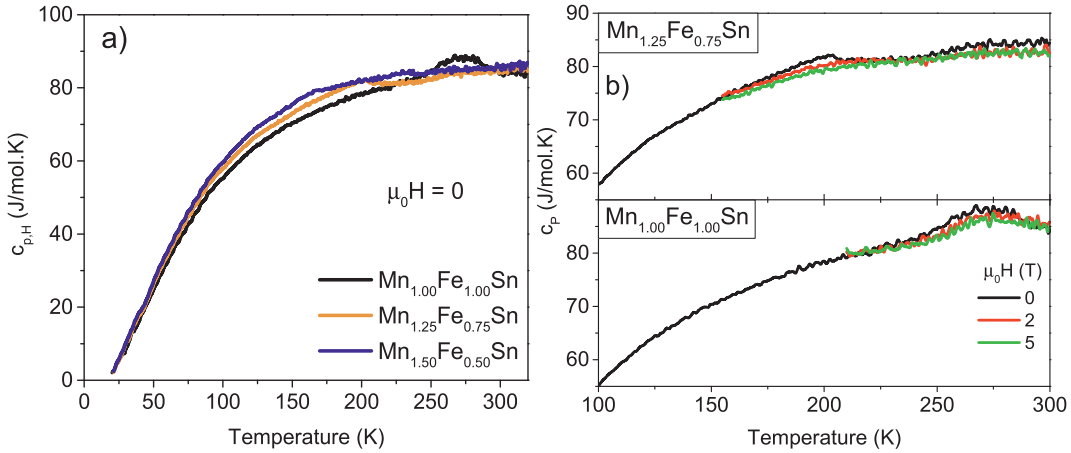

Fig. 6. (a) Specific heat of samples with $y = 0.50$, 0.75 and 1.00 measured with a heat flux setup with a Peltier element at $\mu_0H = 0$. (b) Influence of the magnetic field over the specific heat of samples with $y = 0.75$ and 1.00.

Table 2
Magnetocaloric effect comparison with literature data. All number stands for a magnetic field variation of 2 T (except for the $Mn_{2.4}Fe_{0.6}Sn_2$, which had only 5 T numbers at the reference).

Compound	T_C (K)	$-\Delta S_{Peak}$ (J/kg.K)	RCP (J/kg)	References
Gd	294	4.9	180.8	[51]
$Mn_{2.4}Fe_{0.6}Sn_2$	268/185	3.3 ($\mu_0\Delta H$ = 5 T)	204.2 ($\mu_0\Delta H$ = 5 T)	[52]
$(Mn_{0.55}Fe_{0.45})_5Sn_3$	298/259	1.1	66.1	[11]
$Mn_{1.50}Fe_{0.50}Sn$	177	1.0	88.4	This work
$Mn_{1.25}Fe_{0.75}Sn$	204	1.1	80.2	This work
$Mn_{1.00}Fe_{1.00}Sn$	284	1.0	85.8	This work
$Mn_{0.75}Fe_{1.25}Sn$	383	1.2	85.2	This work

can see that it reaches a reasonable value of 85 J/kg under the moderate 2 T magnetic field change. As the series covers an extensive temperature range, it is possible to consider a multilayer compound or even a possible composite capable of work in such range. Besides that, since these materials present low cost, are easily manufactured, have constant cycling stability and a good temperature span, they can be considered to applications at magnetic refrigeration systems or even thermomagnetic motors.

4. Conclusions

We carried out systematic studies on crystallographic, magnetic, calorimetric and magnetocaloric properties for $Mn_{2-y}Fe_ySn$ alloys. Through the analyses of SEM images, we concluded that our samples are biphasic in the $0.50 \leq y \leq 1.75$ range. EDS semi-quantitative analysis indicated the presence of $Mn_{2-x}Sn$ and Mn_3Sn phases and pointed out that the Fe substitution occurred accordingly with the nominal values, i.e. Fe replaced the same Mn atoms sites, maintaining the 2:1 and 3:1 original stoichiometry. Also, from SEM images and EDS analysis, we observed that $Mn_{2-x}Sn$ phase is predominant in all samples. XRD data were analyzed through Rietveld refinement and the best fitting was reached when the $Mn_{2-x}Sn$ and Mn_3Sn phases were adjusted with Ni_2In and Ni_3Sn-type structures (hexagonal $P6_3/mmc$), respectively. As expected, a monotonic decrease of the lattice parameters *a* and *c* with increasing Fe concentration was observed for both major and minor phases. The quantitative phase analysis, by Rietveld refinement, also pointed out $Mn_{2-x}Sn$ as the major phase, in agreement with SEM and EDS analysis. Magnetization measurements corroborate with the ferrimagnetic behavior showed in previous studies for Mn-Fe-Sn alloys, with an indication of ferromagnetic coupling at the Fe-rich samples leading to an increase of saturation magnetization found at the measured magnetization isotherms. Neutron diffraction investigations, however, are needed to confirm how Fe replacement in Mn sites impacts the magnetic arrangement in each found phase. The series exhibited two transitions where the lower Curie temperature was attributed to the 2:1 phase (T_{C1}) and the higher to the 3:1 phase (T_{C2}). T_{C1} and T_{C2} increased with Fe concentration through all samples. T_{C1} increased from 177 K towards 546 K and T_{C2} increased from 260 K to 704 K. The series transition temperatures are easily adjusted with the right Fe-Mn ratio and they cover a wide range of 369 K (T_{C1}) and 444 K (T_{C2}), including room temperature and its surroundings, which motivated us to the calculation of the magnetocaloric effect for a possible application in magnetic refrigeration. Specific heat measurements where performed and they confirmed the second order character of the magnetic transitions. The magnetic entropy variation results, for the $0.50 \leq y \leq 1.75$, attained values around 1.1 J/kg.K, for a $\mu 0\Delta H$ of 2 T, and the RCP reached a moderate 85 J/kg value. All these combined findings suggest the $Mn_{2-y}Fe_ySn$ series materials as possible candidates for magnetic refrigeration and thermomagnetic motors since these technologies require layered materials to improve their performance.

Declaration of Competing Interest

The authors declare that they have no known competing financial interests or personal relationships that could have appeared to influence the work reported in this paper.

Acknowledgements

The authors are grateful to UNICAMP and Multiuser Central Facilities from UFABC, for the experimental support. M.R. Felez acknowledge to CNPq (153708/2018-2) for scholarship. D.Z. Florio acknowledge to FAPESP (2015/24999-2) and CNPq (309600/2018-9). J.C. B. Monteiro would like to thank CAPES support (88882.315473/2019-01).

References

[1] J. Lyubina, Magnetocaloric materials for energy efficient cooling, J. Phys. D: Appl. Phys. 50 (2017) 053002, , https://doi.org/10.1088/1361-6463/50/5/053002.
[2] T. Mazet, H. Ihou-Mouko, B. Malaman, Mn_3Sn_2: a promising material for magnetic refrigeration, Appl. Phys. Lett. 89 (2006) 1–4, https://doi.org/10.1063/1.2220541.
[3] Q. Recour, T. Mazet, B. Malaman, Magnetocaloric properties of Mn_3Sn_2 from heat capacity measurements, J. Appl. Phys. 105 (2009), https://doi.org/10.1063/1.3074093.
[4] V. Franco, J.S. Blázquez, J.J. Ipus, J.Y. Law, L.M. Moreno-Ramírez, A. Conde, Magnetocaloric effect: from materials research to refrigeration devices, Prog. Mater. Sci. 93 (2018) 112–232, https://doi.org/10.1016/j.pmatsci.2017.10.005.
[5] E. Brück, O. Tegus, D.T.C. Thanh, K.H.J. Buschow, Magnetocaloric refrigeration near room temperature (invited), J. Magn. Magn. Mater. 310 (2007) 2793–2799, https://doi.org/10.1016/j.jmmm.2006.10.1146.
[6] C. Aprea, A. Greco, A. Maiorino, C. Masselli, Magnetic refrigeration: an eco-friendly technology for the refrigeration at room temperature, J. Phys. Conf. Ser. 655 (2015) 012026, , https://doi.org/10.1088/1742-6596/655/1/012026.
[7] S. Lidin, A.-K. Larsson, A survey of superstructures in intermetallic NiAs-Ni_2In-type phases, J. Solid State Chem. 118 (1995) 313–322, https://doi.org/10.1006/jssc.1995.1350.
[8] S. Anzai, S. Fujii, S. Ohta, H. Yoshida, T. Kaneko, R. Sugi, T. Yoshida, M. Matoba, T. Wada, F. Science, Pressure effect on the curie temperature of Ni_2In-type $(Mn_{1-z}Fez)_7Sn_4$, Rev. High Press. Sci. Technol. 7 (1998) 547–549.
[9] H. Shiraishi, T. Hori, N. Ohkubo, K. Ohoyama, Magnetic and neutron diffraction study on Ni_2In type $(Mn_{1-x}Fe_x)_{65}Sn_{35}$, Phys. Status Solidi 1 (2004) 3660–3663, https://doi.org/10.1002/pssc.200405527.
[10] V.A. Virchenko, T.M. Tkachenko, M.F. Thomas, Temperature features of the magnetic interactions in manganese stannide, Low Temp. Phys. 33 (2007) 833–838, https://doi.org/10.1063/1.2746856.
[11] J.H. Xu, X.M. Liu, Y.H. Xia, W.Y. Yang, H.L. Du, J.B. Yang, Y. Zhang, Y.C. Yang, Magnetic properties and magnetocaloric effect of $(Mn_{1-x}Fe_x)_5Sn_3$ (x = 0–0.5) compounds, J. Appl. Phys. 113 (2013) 17A921, , https://doi.org/10.1063/1.4798308.
[12] R. Fuglsby, P. Kharel, W. Zhang, S. Valloppilly, Y. Huh, D.J. Sellmyer, Magnetism of hexagonal Mn 1.5 X 0.5 Sn (X = Cr, Mn, Fe, Co) nanomaterials, J. Appl. Phys. 117 (2015) 17D115, https://doi.org/10.1063/1.4913821.
[13] A. Dianoux, B. Malaman, T. Mazet, Magnetic and magnetocaloric properties of $Fe_{5-x}Mn_xSn_3$, Solid State Commun. 260 (2017) 40–44, https://doi.org/10.1016/j.ssc.2017.05.012.
[14] K. Murakami, M. Nemoto, Some Experiments and considerations on the behavior of thermomagnetic motors, IEEE Trans. Magn. 8 (1972) 387–389, https://doi.org/10.1109/TMAG.1972.1067406.
[15] D. Solomon, Thermomagnetic mechanical heat engines, J. Appl. Phys. 65 (1989) 3687–3693, https://doi.org/10.1063/1.342595.
[16] A. Karle, The thermomagnetic Curie-motor for the conversion of heat into mechanical energy, Int. J. Therm. Sci. 40 (2001) 834–842, https://doi.org/10.1016/S1290-0729(01)01270-4.
[17] M. Trapanese, A. Viola, V. Franzitta, Design and experimental test of a thermomagnetic motor, AASRI Proc. 2 (2012) 199–204, https://doi.org/10.1016/j.aasri.2012.09.035.
[18] C.S. Alves, F.C. Colman, G.L. Foleiss, G.T.F. Vieira, W. Szpak, Numerical simulation and design of a thermomagnetic motor, Appl. Therm. Eng. 61 (2013) 616–622, https://doi.org/10.1016/j.applthermaleng.2013.07.053.
[19] L.D.R. Ferreira, C.V.X. Bessa, I. Silva, S. Gama, A linear reciprocating thermomagnetic motor powered by water heated using solar energy, Green Des. Mater. Manuf. Process. CRC Press, 2013, pp. 107–111, , https://doi.org/10.1201/b15002-23.
[20] L.D.R. Ferreira, C.V.X. Bessa, I. Da Silva, S. Gama, A heat transfer study aiming optimization of magnetic heat exchangers of thermomagnetic motors, Int. J. Refrig. 37 (2014) 209–214, https://doi.org/10.1016/j.ijrefrig.2013.09.010.
[21] M. Trapanese, G. Cipriani, V. Di Dio, V. Franzitta, A. Viola, Optimization of a thermomagnetic motor, J. Appl. Phys. 117 (2015) 17A750, https://doi.org/10.1063/1.4919231.
[22] A. Kitanovski, U. Plaznik, J. Tušek, A. Poredoš, New thermodynamic cycles for

magnetic refrigeration, Int. J. Refrig. 37 (2014) 28–35, https://doi.org/10.1016/j.ijrefrig.2013.05.014.
[23] R. Bjørk, C.R.H. Bahl, K.K. Nielsen, The lifetime cost of a magnetic refrigerator, Int. J. Refrig. 63 (2016) 48–62, https://doi.org/10.1016/j.ijrefrig.2015.08.022.
[24] A. Rowe, A. Tura, Experimental investigation of a three-material layered active magnetic regenerator, Int. J. Refrig. 29 (2006) 1286–1293, https://doi.org/10.1016/j.ijrefrig.2006.07.012.
[25] M.R. Felez, A.A. Coelho, S. Gama, Magnetic properties of $Mn_{3-x}Fe_xSn$ compounds with tuneable Curie temperature by Fe content for thermomagnetic motors, J. Magn. Magn. Mater. 444 (2017) 280–283, https://doi.org/10.1016/j.jmmm.2017.08.028.
[26] Y. Bao, H. Shen, Y. Huang, D. Xing, H. Wang, M. Phan, Table-like magnetocaloric behavior and enhanced cooling ef fi ciency of a Bi-constituent Gd alloy wire-based composite, J. Alloys Compd. 764 (2018) 789–793, https://doi.org/10.1016/j.jallcom.2018.06.067.
[27] L. Zhou, Y. Tang, Y. Chen, H. Guo, W. Pang, X. Zhao, Table-like magnetocaloric effect and large refrigerant capacity of composite magnetic refrigerants based on $LaFe_{11.6}Si_{1.4}H_y$ alloys, J. Rare Earths. 36 (2018) 613–618, https://doi.org/10.1016/j.jre.2018.01.009.
[28] X.C. Zhong, X.Y. Shen, H.Y. Mo, D.L. Jiao, Z.W. Liu, W.Q. Qiu, H. Zhang, R.V. Ramanujan, Table-like magnetocaloric effect and large refrigerant capacity in $Gd_{65}Mn_{25}Si_{10}$-Gd composite materials for near room temperature refrigeration, Mater. Today Commun. 14 (2018) 22–26, https://doi.org/10.1016/j.mtcomm.2017.12.005.
[29] H. Okamoto, Mn-Sn (manganese-Tin), J. Phase Equilib. (1999).
[30] K. Yasukochi, K. Kanematsu, T. Ohoyama, Magnetic properties of intermetallic compouds in manganese-tin system:$Mn_{3.67}Sn$, $Mn_{1.77}Sn$, and $MnSn_2$, J. Phys. Soc. Jpn. 16 (1961) 1123–1130.
[31] K.H.J. Buschow, P.G. van Engen, R. Jongebreur, Magneto-optical properties of metallic ferromagnetic materials, J. Magn. Magn. Mater. 38 (1983) 1–22.
[32] M. Elding-ponten, L. Stenberg, A. Larsson, S. Lidin, K. Stahl, Three NiAs–Ni_2In type structures in the Mn–Sn system, J. Solid State Chem. 129 (1997) 231–241.
[33] M. Stange, H. Fjellvåg, S. Furuseth, B.C. Hauback, Crystal structure and phase relations for Mn_3Sn_2 and non-stoichiometric $Mn_{2-x}Sn$, J. Alloys Compd. 259 (1997) 140–144, https://doi.org/10.1016/S0925-8388(97)00050-9.
[34] J.S. Kouvel, Exchange anisotropy and long-range magnetic order in the mixed intermetallic compounds, $(Mn, Fe)_3Sn$, J. Appl. Phys. 36 (1965) 980–981, https://doi.org/10.1063/1.1714287.
[35] E. Krén, J. Paitz, G. Zimmer, É. Zsoldos, Study of the magnetic phase transformation in the Mn_3Sn phase, Phys. B + C 80 (1975) 226–230, https://doi.org/10.1016/0378-4363(75)90066-2.
[36] H.C. Walker, L. Szunyogh, K.H. Lee, J.-G. Park, V. Sechovský, H. Cho, A. Deák, P. Park, D. Adroja, K. Uhlířová, J. Jackson, H.-L. Kim, J. Oh, Magnetic excitations in non-collinear antiferromagnetic Weyl semimetal Mn_3Sn, NPJ Quantum Mater. 3 (2018), https://doi.org/10.1038/s41535-018-0137-9.
[37] K. Manna, Y. Sun, L. Muechler, J. Kübler, C. Felser, Heusler, Weyl and Berry, Nat. Rev. Mater. 3 (2018), https://doi.org/10.1038/s41578-018-0036-5.
[38] T. Higo, R. Arita, O.M.J. van't Erve, R.D. Shull, J. Orenstein, Y.P. Kabanov, L. Wu, T. Koretsune, S. Patankar, D.B. Gopman, Y. Li, S. Nakatsuji, D. Rees, H. Man, C.L. Chien, M.-T. Suzuki, M. Ikhlas, Large magneto-optical Kerr effect and imaging of magnetic octupole domains in an antiferromagnetic metal, Nat. Photon. 12 (2018) 73–78, https://doi.org/10.1038/s41566-017-0086-z.
[39] T. Nagamiya, S. Tomiyoshi, Y. Yamaguchi, Triangular spin configuration and weak ferromagnetism of Mn_3Sn and Mn_3Ge, Solid State Commun. 42 (1982) 385–388, https://doi.org/10.1016/0038-1098(82)90159-4.
[40] J.W. Cable, N. Wakabayashi, P. Radhakrishna, Magnetic excitations in the triangular antiferromagnets Mn_3Sn and Mn_3Ge, Phys. Rev. B 48 (1993) 6159–6166, https://doi.org/10.1103/PhysRevB.48.6159.
[41] W.J. Feng, D. Li, W.J. Ren, Y.B. Li, W.F. Li, J. Li, Y.Q. Zhang, Z.D. Zhang, Structural magnetic and transport properties of $Mn_{3.1}Sn_{0.9}$ and $Mn_{3.1}Sn_{0.9}N$ compounds, J. Alloys Compd. 437 (2007) 27–33, https://doi.org/10.1016/j.jallcom.2006.07.106.
[42] S. Nakatsuji, N. Kiyohara, T. Higo, Large anomalous Hall effect in a non-collinear antiferromagnet at room temperature, Nature 527 (2015) 212–215, https://doi.org/10.1038/nature15723.
[43] T.F. Duan, W.J. Ren, W.L. Liu, S.J. Li, W. Liu, Z.D. Zhang, Magnetic anisotropy of single-crystalline Mn_3Sn in triangular and helix-phase states, Appl. Phys. Lett. 107 (2015), https://doi.org/10.1063/1.4929447.
[44] X. Li, L. Xu, L. Ding, J. Wang, M. Shen, X. Lu, Z. Zhu, K. Behnia, Anomalous Nernst and Righi-Leduc effects in Mn_3Sn: berry curvature and entropy flow curvature and entropy flow, Phys. Rev. Lett. 119 (2017) 056601, , https://doi.org/10.1103/PhysRevLett.119.056601.
[45] M. Ikhlas, T. Tomita, T. Koretsune, M.-T. Suzuki, D. Nishio-Hamane, R. Arita, Y. Otani, S. Nakatsuji, Large anomalous Nernst effect at room temperature in a chiral antiferromagnet, Nat. Phys. 13 (2017) 1085–1090, https://doi.org/10.1038/nphys4181.
[46] Y. Li, Y. Otani, S. Nakatsuji, T. Higo, C.L. Chien, D. Qu, Anomalous Hall effect in thin films of the Weyl antiferromagnet Mn_3Sn, Appl. Phys. Lett. 113 (2018) 202402, , https://doi.org/10.1063/1.5064697.
[47] A.L. Balk, N.H. Sung, S.M. Thomas, P.F.S. Rosa, R.D. McDonald, J.D. Thompson, E.D. Bauer, F. Ronning, S.A. Crooker, Comparing the anomalous Hall effect and the magneto-optical Kerr effect through antiferromagnetic phase transitions in Mn_3Sn, Appl. Phys. Lett. 114 (2019), https://doi.org/10.1063/1.5066557.
[48] A.H. MacDonald, P.K. Muduli, Y. Omori, M. Kimata, T. Tomita, Y. Otani, M. Ikhlas, S. Sugimoto, H. Chen, K. Kondou, S. Nakatsuji, Magnetic and magnetic inverse spin Hall effects in a non-collinear antiferromagnet, Nature 565 (2019) 627–630, https://doi.org/10.1038/s41586-018-0853-0.
[49] A. Nelson, Y. Huh, P. Kharel, V.R. Shah, R. Skomski, D.J. Sellmyer, Structural, magnetic, and electron transport properties of $Mn_{3-x}Pt_xSn$ ($x = 0, 0.5, 1$) nanomaterials, J. Appl. Phys. 115 (2014) 17A923, https://doi.org/10.1063/1.4865977.
[50] J.C.B. Monteiro, R.D. dos Reis, F.C.G. Gandra, N.R. Dilley, Determination of the magnetocaloric properties using a PPMS, Quantum Des. (2014).
[51] J.C.B. Monteiro, R.D. dos Reis, A.M. Mansanares, F.G. Gandra, Determination of the magnetocaloric entropy change by field sweep using a heat flux setup, Appl. Phys. Lett. 105 (2014) 074104, , https://doi.org/10.1063/1.4894004.
[52] Q. Recour, T. Mazet, B. Malaman, Magnetic and magnetocaloric properties of $Mn_{3-x}Fe_xSn_2$ ($0.1 \leqslant x \leqslant 0.9$), J. Phys. D: Appl. Phys. 41 (2008) 185002, , https://doi.org/10.1088/0022-3727/41/18/185002.
[53] K.A. Gschneidner, V.K. Pecharsky, Magnetocaloric materials, Annu. Rev. Mater. Sci. 30 (2000) 387–429, https://doi.org/10.1146/annurev.matsci.30.1.387.
[54] K.A. Gschneidner Jr., V.K. Pecharsky, A.O. Pecharsky, C.B. Zimm, Recent developments in magnetic refrigeration, Mater. Sci. Forum 315–317 (1999) 69–76, https://doi.org/10.4028/www.scientific.net/MSF.315-317.69.